fluids

MDPI

Article

Conceptual Design of a UVC-LED Air Purifier to Reduce Airborne Pathogen Transmission—A Feasibility Study

Saket Kapse [1], Dena Rahman [2], Eldad J. Avital [2,*], Nithya Venkatesan [1], Taylor Smith [2], Lidia Cantero-Garcia [2], Fariborz Motallebi [2], Abdus Samad [3] and Clive B. Beggs [4]

[1] School of Electrical Engineering, Vellore Institute of Technology, Chennai 600077, India
[2] School of Engineering and Materials Science, Queen Mary University of London, London E1 4NS, UK
[3] Department of Ocean Engineering, Indian Institute of Technology, Madras 300036, India
[4] Carnegie School of Sport, Leeds Beckett University, Leeds LS6 3QS, UK
* Correspondence: e.avital@qmul.ac.uk

Abstract: Existing indoor closed ultraviolet-C (UVC) air purifiers (UVC in a box) have faced technological challenges during the COVID-19 breakout, owing to demands of low energy consumption, high flow rates, and high kill rates at the same time. A new conceptual design of a novel UVC-LED (light-emitting diode) air purifier for a low-cost solution to mitigate airborne diseases is proposed. The concept focuses on performance and robustness. It contains a dust-filter assembly, an innovative UVC chamber, and a fan. The low-cost dust filter aims to suppress dust accumulation in the UVC chamber to ensure durability and is conceptually shown to be easily replaced while mitigating any possible contamination. The chamber includes novel turbulence-generating grids and a novel LED arrangement. The turbulent generator promotes air mixing, while the LEDs inactivate the pathogens at a high flow rate and sufficient kill rate. The conceptual design is portable and can fit into ventilation ducts. Computational fluid dynamics and UVC ray methods were used for analysis. The design produces a kill rate above 97% for COVID and tuberculosis and above 92% for influenza A at a flow rate of 100 L/s and power consumption of less than 300 W. An analysis of the dust-filter performance yields the irradiation and flow fields.

Keywords: air purifier; UVC disinfection; fluid dynamics; airborne disease

Citation: Kapse, S.; Rahman, D.; Avital, E.J.; Venkatesan, N.; Smith, T.; Cantero-Garcia, L.; Motallebi, F.; Samad, A.; Beggs, C.B. Conceptual Design of a UVC-LED Air Purifier to Reduce Airborne Pathogen Transmission—A Feasibility Study. *Fluids* **2023**, *8*, 111. https://doi.org/10.3390/fluids8040111

Academic Editors: Kambiz Vafai and D. Andrew S. Rees

Received: 25 December 2022
Revised: 13 March 2023
Accepted: 22 March 2023
Published: 27 March 2023

1. Introduction

1.1. Motivation and Aims

The COVID-19 pandemic has highlighted the need to control indoor air quality and reduce the concentration of aerosolized pathogens in room air. Not only has the pandemic raised awareness of the dangers posed by aerosols containing the SARS-CoV-2 virus [1,2], but it has also highlighted the threat posed by other airborne diseases, such as tuberculosis (TB) [3,4], measles [5], and influenza [6]. These diseases, although over-shadowed by COVID-19 in recent years, still represent a major public health threat, with, for example, about a quarter of the global population estimated to have been infected with TB [7]. TB is a major problem in South Asia, with India in particular accounting for 26% of all cases globally in 2020 [8]. As such, there is a pressing need to develop low-cost public health interventions to protect people against the transmission of airborne disease in countries like India.

COVID-19, TB, measles, and influenza are all diseases known to be transmitted by the airborne route [1,9,10]. Individuals with these diseases can be highly infectious and may shed viral particles and bacteria in large numbers via respiratory aerosols. The fate of pathogens emitted during coughing, sneezing, talking, and breathing depends very much on the initial sizes of the respiratory particles exhaled [11]. Respiratory pathogens exhaled in large droplets (>100 microns) tend to behave ballistically and may hit the face (or food)

of another person [12] in close proximity (<2 m), in which case social distancing and the use of screens can significantly reduce transmission [13]. However, respiratory pathogens exhaled in smaller droplets (<100 microns) can potentially travel much further. This is because droplets of this size rapidly evaporate to become aerosols (<20 microns) [14], which linger in the air [12,15] and potentially infect people at longer distances. Such fine aerosols can also be transmitted via poorly maintained mechanical ventilation and air-conditioning systems that re-circulate the air and thus have the potential to spread airborne disease [16].

Given the collective threat posed by airborne disease, the provision of adequate room ventilation is essential to reduce the pathogen load in the air [12,13], particularly in spaces where large numbers of people tend to congregate [17]. However, this is not always possible because many existing spaces have poorly designed, inadequate ventilation systems that are difficult to upgrade. Furthermore, there is an additional problem that inclement weather conditions (both hot and cold) may prevent the opening of windows or the use of full 'fresh air' mechanical ventilation, which causes a negative impact on energy consumption and the comfort of occupants.

In such scenarios, the use of supplementary air-cleaning devices known as high-efficiency particulate air (HEPA) filters can help [18]. HEPA filters are designed to remove particles as small as 0.3 microns with an efficiency of 99.95% and can be mounted either inside a heating, ventilating, and air conditioning (HVAC) system [13] or inside a stand-alone room-mounted air purifier, drawing air from the room using a fan and then capturing airborne particles before blowing the cleaned air back into the room [18]. However, such filters require regular maintenance and replacement and are not well suited to dry, dusty environments, such as those found in India, where HEPA filters may rapidly clog. Dust and other particulate matter collecting on the HEPA filter create high resistance to airflow, causing both increased energy consumption and a reduction in the clean air delivery rate (CADR). Hence, alternative technologies, such as ultraviolet-C (UVC) light and air ionization with self-cleaning filter technologies, which do not suffer from this problem, are currently being pursued.

UVC light of wavelength 220–280 nm is known to damage the genetic material (DNA or RNA) of pathogens (viruses or bacteria) and prevent them from causing infection [10]. At these wavelengths, photons of light break the hydrogen bonds in the nucleic material to form pyrimidine dimers, which means that genetic replication of the pathogen cannot occur [19]. UV air disinfection has been implemented since the 1930s to mitigate the spread of TB [20], with open UVC lamps radiating light above people's heads of room occupants (i.e., upper-room UVC air disinfection) generally being the favored configuration [13].

Recently, it has been suggested that upper-room UVC air disinfection may be effective at mitigating the spread of the SARS-CoV-2 virus in aerosols, e.g., [10,21]. The SARS-CoV-2 virus appears to be particularly vulnerable to damage from UVC light when in aerosols [10]. However, because the irradiation field is open, the UVC lamps must be shielded from the downward view by baffles, which reduces the intensity of the upper-room UVC field. Furthermore, care must be taken to prevent UVC light from being reflected into the lower room space in order to keep people within the safety limits of UVC light intensity exposure [20]. Such installation also requires ceiling fans to promote good mixing of air between the lower and the upper zones so the residence time of the aerosol droplets in the upper-room irradiation zone is maximized. Hence, upper-room UVC systems are more suitable for large public indoor places with high ceilings, such as schools, hospitals, and transport hubs, where the installation costs can be well justified.

Air disinfection can also be achieved by mounting UVC lamps inside a 'box' with a fan, which allows the technology to act as a stand-alone air purifier that can be safely mounted in a room or inside a duct of a mechanical ventilation system [22]. The design is similar to a HEPA filter, but a UVC chamber replaces a HEPA filter in this design. A UVC-based purifier is compact and avoids damaging eyes and skin [23,24] as the UVC light is shielded inside the box. As such, these devices are well suited to domestic, small-business, and rural

applications, where the capital expense of installing upper-room UV air disinfection may be prohibitively high.

However, 'UV in a box' type devices present major technological challenges because it is difficult to achieve sufficient residence time for the pathogens to be inactivated inside the UVC chamber while maintaining a reasonable air flow rate at an acceptable financial cost and power consumption. This is a major technological challenge because it can undermine such devices' effectiveness as an infection control intervention. Unfortunately, many wrongly assume that such devices protect room occupants from acquiring airborne infection because a device can achieve a 99.9% disinfection rate based on a 'single-pass' microbiological test. However, such claims can be highly misleading because they relate purely to the air that passes through the UV device and not to the overall effect that the unit has on the room space. The design is primarily dictated by the volume flow rate at which the disinfected air is supplied to the space (i.e., the CADR) [25]. This is highlighted in Equation (1), showing the steady-state concentration achieved by an air-cleaning device in a fully mixed room space:

$$C = \frac{q}{\dot{v}_r + \dot{v}_{ac}\eta} \quad (1)$$

where C is the contaminant concentration in the room space under steady-state conditions (virions/m^3), q is the steady-state room contamination rate (virions/s), $\dot{v}_r$ is the room ventilation flow rate (m^3/s), $\dot{v}_{ac}$ is the air flow rate through the UVC air purifier (m^3/s), and η is the single-pass efficiency of the air disinfection device expressed as a fraction.

Equation (1) shows that the air-cleaning device is unlikely to significantly impact the transmission of viruses within a room space unless the device can deliver a relatively high airflow rate. From an infection control standpoint, it is much better to install a less efficient device that delivers a large quantity of 'almost disinfected' air rather than having a small device providing very clean air with a low flow rate. So, the technical challenge is supplying as much clean air as possible to the room space while still maintaining a relatively high level of disinfection and not consuming large amounts of energy.

One low-energy technology that appears to have potential in this respect is the light-emitting diode (LED). Recently, LEDs emitting UVC light with a wavelength of 279 nm have been developed. These do not ionize the air and therefore produce no ozone, and they are potentially more efficient in terms of power radiating over short distances compared with conventional low-pressure lamps at 254 nm. LEDs also have the advantages of compactness and no mercury used in their production [26].

In this paper, a novel, low-energy 'UVC in a box' air purifier is presented, which has been specifically designed for use in low- and medium-income countries, where cost constraints are a major obstacle to implementation. This necessitates a compromise between delivering the maximum amount of disinfected air and ensuring that the single-pass efficiency of the device is high while still maintaining low energy consumption. As such, the development team set a target of achieving a CADR of 100 L/s with a 95% inactivation rate against the SARS-CoV-2 virus. This is an equivalent ventilation rate of six air changes per hour (ACH) in a large living room or mid-size office room of $6 \times 4 \times 2.5$ m^3, which is WHO's minimum requirement for a health setting where no aerosol-generating procedure occurs [27]. It can also support up to ten people with 10 L/s per person equivalent ventilation, which follows WHO's recommendation for non-residential buildings [27]. The LED layout, together with a new aerodynamic design, is optimized so that the aerosol droplets are sufficiently exposed to the UVC field. This analysis is presented in the paper.

1.2. The Conceptual Design

The concept of the air purifier is illustrated in Figure 1. An axial fan draws air through an irradiation chamber comprising four opposite-facing banks of LEDs emitting light at 279 nm mounted in two cells. Keys to the design are (i) a novel turbulence-generating grid that mixes the air in the irradiation chamber, thus ensuring maximum exposure time, and

(ii) an optimal LED layout to reduce power consumption and manufacturing costs while achieving the required inactivation rate of pathogens.

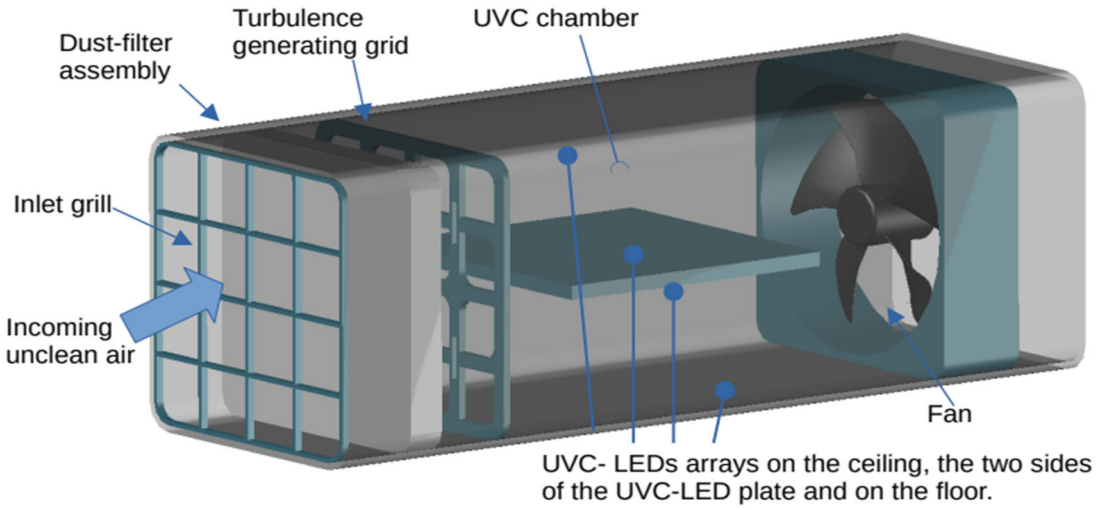

(**a**)

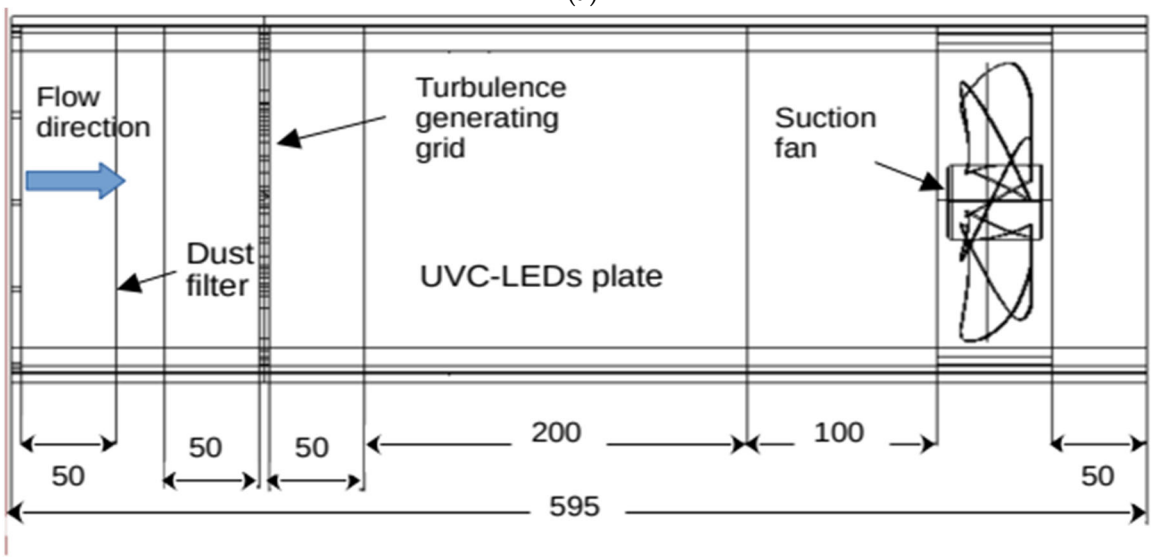

(**b**)

Figure 1. Conceptual design of the UVC-LED air purifier in (**a**) isometric view and (**b**) longitudinal cross-section, where all units are in mm.

Dust accumulation in the device can impair the LED efficiency. A low-cost coarse-dust filter is mounted in front of the UVC chamber to capture particles larger than 10 microns in diameter. Most infectious droplet sizes are in the range of 2 to 20 microns [28]; thus, the filter may become clogged and contaminated over time. To facilitate the safe replacement of the filter, an isolating 'cassette' assembly is used with the dust filter residing between the two sets of louvers (as illustrated in Figure 2). The louvers are opened when the cassette is slotted into the air-cleaning device and are closed when the cassette is removed for cleaning.

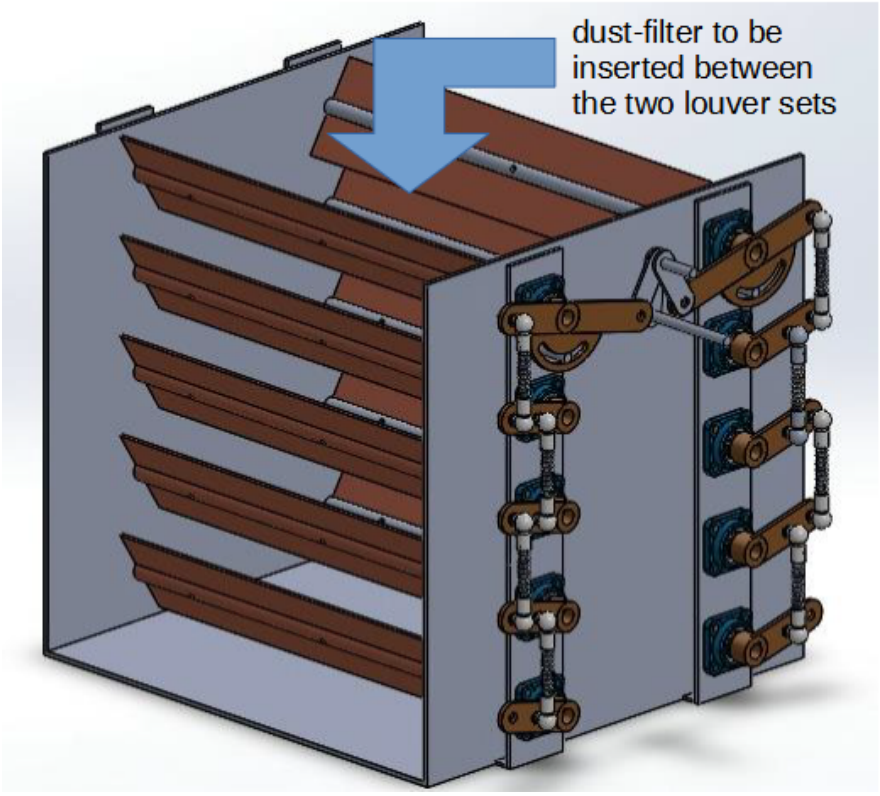

Figure 2. Conceptual design of the louvers 'cassette' assembly to provide safe removal of the dust filter. The louvers are closed for the filter's replacement; the all 'cassette' assembly is pulled out from the air purifier, and the filter can be safely removed.

The air passes through the dust filter, the turbulence-generating grids, the UVC chamber, and the suction fan sequentially. The indicative axial lengths of the device elements are illustrated in Figure 1b. Settling distances were taken from one element to the other. The overall cross-sectional area is 20×20 cm^2 so that it can work as a stand-alone air purifier or as an air purifier for ventilation ducts. This yields a bulk velocity of 2.5 m/s for a flow rate of 100 L/s. However, the bulk velocity increases when the cross-section narrows in the turbulence-generating grid.

2. Methodology

The methodology is divided into three categories: (i) conventional electrical–mechanical design that leads to the concept discussed in Section 1.2, (ii) aerodynamic study, and (iii) LED disinfection study. The novelty in this research is within the design of the UVC chamber in terms of the LED layout and the turbulence-generating grid, and this is the focus of this section.

2.1. Aerodynamic Methodology

Both one-dimensional (1D) and three-dimensional (3D) analyses were carried out. The 3D analysis was based on computational fluid dynamics (CFD). The dust filter's pressure drop and efficiency were calculated using 1D analysis.

The pressure drop Δp over the dust filter can be modeled as a netted fibrous filter [29]:

$$\Delta p = 64 \mu U_0 h \left(\frac{\alpha_f}{d_f^2} + \frac{\alpha_p}{d_p^2} \right)^{1/2} \left(\frac{\alpha_f}{d_f} + \frac{\alpha_p}{d_p} \right) \quad (2)$$

where α_f and α_p are the fiber- and particle-packing relative densities (solidities), respectively, and d_f and d_p are the cylindrical-fiber and spherical-particle diameters, respectively.

For the present dust filter, $\alpha_f = 0.05$, following a previous study on fibrous filters [30]. When $\alpha_p = 0$, the filter is clean; as α_p increases, the filter becomes more clogged, and hence, Δp increases. The pressure drop Δp is linearly proportional to the air's dynamic viscosity μ and the incoming air speed U_0, and thus, Stokes flow is assumed around the fibers. h is the thickness of the filter.

The clean filter efficiency E is calculated as [30]

$$E = 1 - e^{\frac{-4\alpha_p E_T h}{\pi(1-\alpha_p)d_f}} \tag{3}$$

The procedure to calculate the total single fiber efficiency (SFE) E_T is given in Appendix A. Again, Stokes flow was assumed around the fibers.

The louvers, mounted in front and after the filter, cause a pressure drop (Δp_g) and can be modeled as grids in a similar way as the turbulence-generating grid. The following 1D approximation was derived for a netted grid at a moderate-to-high Reynolds number ($Re_{\mathrm{df}} > 1000$), which is justified by the centimeter scale of the grid elements [31];

$$\Delta p_g \simeq 0.52\rho U_0^2 \left[\frac{1}{(1-\alpha_g)^2} - 1 \right] \tag{4}$$

where ρ is the air density and α_g is the grid solidity. The louvers have solidities much lower than 0.5, and thus, their pressure drop should be less than the dynamic pressure $\rho U_0^2/2$.

The skin friction over the device walls and the UVC chamber plates also causes a pressure drop.

Assuming fully developed turbulent flow in a non-circular (square) pipe, then the pressure drop Δp_d due to the entire length of the device, $L \simeq 0.6$ m can be estimated as [32]

$$\frac{\Delta p_d}{L} = \frac{1}{2}\frac{\lambda}{d_h}\rho U_0^2 \tag{5}$$

where d_h is the hydraulic diameter, which is 0.2 m for our square cross-section. λ is the resistance coefficient, which is about 2.5 for the Reynolds number $\mathrm{Re} = U_0 d_h/v = 3.38 \times 10^4$ [32], yielding $\Delta p_d \simeq 30$ Pa. This low pressure drop, as compared to the dust filter, is confirmed by the CFD analysis discussed later.

The CFD is based on the RANS approach and the standard k-omega SST model that is suitable for transitional flows. Incompressible flow is assumed because of the low speed of the flow. The commercial software Ansys is used along with a second-order upwind scheme for the convective terms and a second-order central scheme for the diffusion terms. The SIMPLE approach is used for the iteration until achieving converged solutions in all solved equations: continuity, momentum, and the RANS model's two equations. No slip-wall boundary conditions are applied on the inner walls of the device along the standard wall function for the RANS model. Further details on such RANS computations and the k-omega model can be found in various textbooks and studies, e.g., [33,34]. An inflow velocity of $U_0 = 2.5$ m/s is imposed for the inlet cross-section area of 20 × 20 cm to provide a flow rate of 100 L/s. An unstructured computational mesh is applied along with grid refinement near the grid, generating turbulence. Grid convergence is checked for the flow properties discussed in Section 3.

2.2. UVC Disinfection Methodology

The inactivation of the aerosolized pathogens in a UVC field with irradiance S (W/m^2) can be modeled as [7]

$$\frac{N(t)}{N(t=0)} = e^{-Z*S*t} \tag{6}$$

where N is the number of active pathogens; Z is the inactivation of constant, which is specific for the pathogen and the surrounding medium (m^2/J); and t is the residence time

(s) of the pathogen in the UVC field. The inactivation constants are given in Table 1. A larger value of Z implies the pathogen disinfection rate is higher.

Table 1. Inactivation constants Z in aerosol [7].

Pathogen	Z (m^2/J)
SARS-CoV-2	0.377
Mycobacterium tuberculosis	0.472
Influenza A	0.270

The irradiance S is calculated using the $\cos^3\theta$ law that assumes an inverse square distance law, i.e., neglecting scattering and absorption by the air [35]. This is justified by the short distance of radiation of up to 10 cm. Reflections from surfaces that can enhance the irradiance are also neglected and are left for future study. Considering the LED lamp as a point source mounted on the plate, as shown in Figure 1, then, at a vertical distance h_p from the plate and at a polar angle θ from the vertical line,

$$S = \frac{I_0 P(\theta) \cos^3\theta}{h_p^2} \tag{7}$$

where I_0 can be calculated by taking S = 3.75 mW/cm^2 at h_p = 2 cm just above the LED lamp [35]. The source directivity $P(\theta)$ is [35]

$$P(\theta) = -2 \times 10^{-6}\theta^3 - 7 \times 10^{-5}\theta^2 + 3 \times 10^{-3}\theta + 0.9614 \tag{8}$$

If $P(\theta) < 0$, then $P(\theta)$ is set to zero. The contributions from different LED lamps are superimposed, assuming constructive interaction.

3. Results and Discussion

The clean dust-filter efficiency E according to Equation (2) is plotted in Figure 3a, showing excellent efficiency for $\alpha_f = 0.05$ and a particle size larger than 12 microns. However, one should note that the Reynolds number of the fiber is about 10, and thus, Stokes flow does not strictly apply. Nevertheless, Stokes drag law still can give an acceptable estimate in that range [36], and hence, the filter with d_f = 50 microns was chosen. The filter's pressure drop is shown in Figure 3b, where clogging, as expressed by the particle's solidity α_p, is seen to significantly increase the pressure drop, indicating the importance of an easy replacement of the inexpensive dust filter, as discussed earlier. As the filter does not capture particles smaller than ~12 microns, the particle's clogging can be allowed up to about $\alpha_p = 0.05$, as the chosen fan can overcome up to 200 Pa pressure drop at a power consumption of about 35 W.

The dust filter effectively stops particles large than 12 microns, which is more than 90% of the volume of a typical household [37]. However, most of the infectious airborne particles are 1 µm $< d_p <$ 20 µm [28], and those must be inactivated by the UVC chamber. To achieve sufficient irradiation while having reasonable power consumption, a staggered offset was applied between the upper and low LED banks, as well as between the LED rows in each bank, leading to the staggered layout given in Figure 4. A staggered layout of UVC lamps is also suggested for water UVC disinfection in open channel flow [38]. Here, such configuration is adapted and modified for air disinfection using multiple layouts and staggering, not just in the rows on the same plane (layout) but also between the layouts, as illustrated in Figure 4. The chamber is split into two chambers so the distance between the two UVC layouts is no more than 10 cm in order to seek the appropriate UVC irradiance field. The UVC chamber is just 20 cm long, and the LEDs rows occupy a spanwise length of 18 cm. The vertical distance between the upper and lower LED banks is 10 cm, and thus,

two irradiation cells in the UVC chamber have an overall cross-section of 20 × 20 cm. This yields 344 LEDs and a power consumption of 258 W.

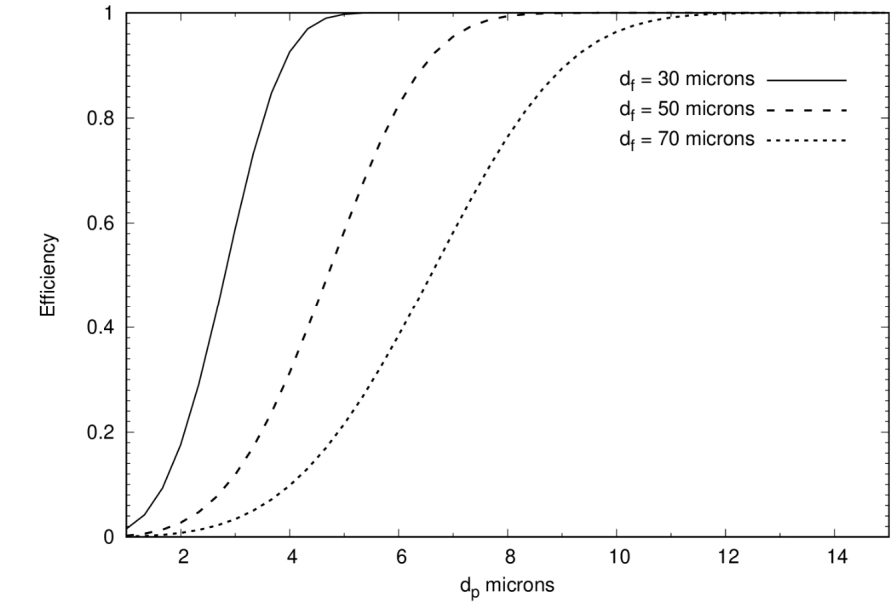

(**a**)

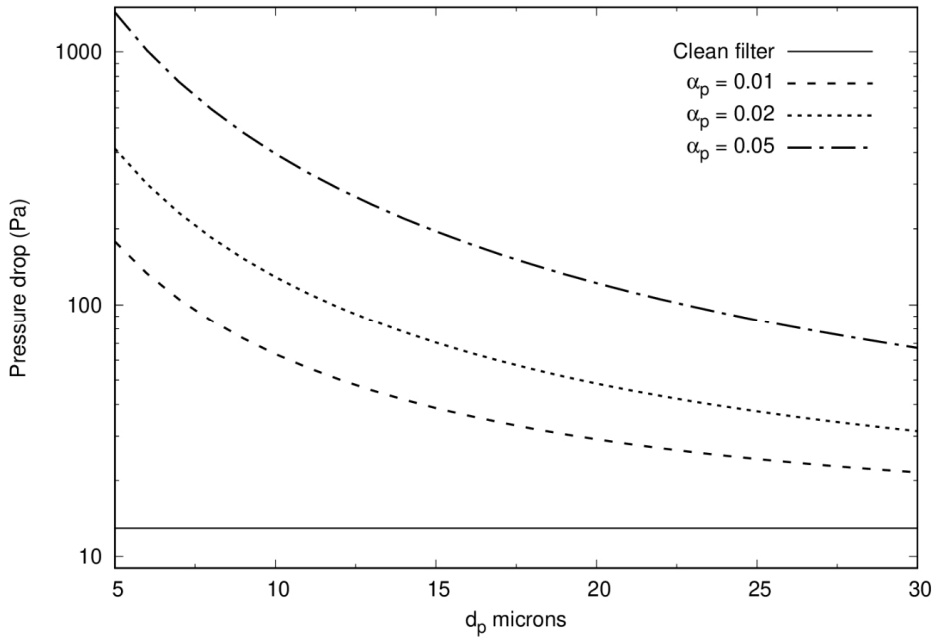

(**b**)

Figure 3. The dust filter's (**a**) efficiency E for several fiber diameters d_f from Equation (3) and (**b**) pressure drop Δp for d_f = 50 microns and several clogging conditions measured by the particle solidity on the filter α_p using Equation (2), where the filter's solidity is $\alpha_f = 0.05$.

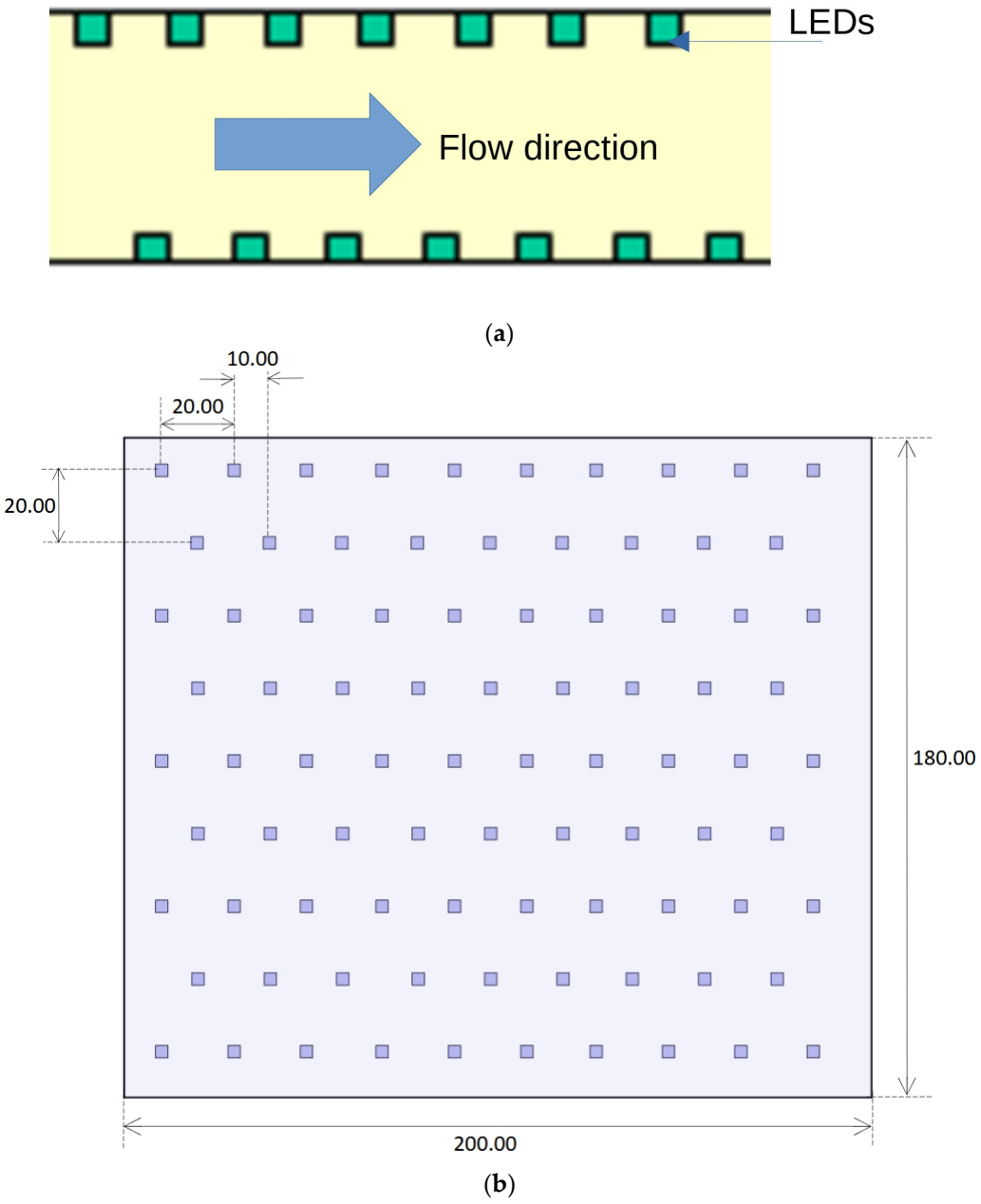

Figure 4. The UVC chamber LEDs layout where (**a**) staggering is arranged between the upper and lower LEDs arrays and (**b**) staggering is also shown in the LED array itself to reduce the number of LEDs. The length unit is mm.

The irradiance contours, as emitted just by the upper LEDs plate and at distances of 4 and 6 cm, are shown in Figure 5, with the highest level around the center, as constructive superposition is assumed between the LEDs. The averaged irradiance per plane in a passage is given in Table 2, where constructive interaction is assumed between the upper and lower LEDs irradiance. This yields theoretical inactivation rates of >97%, >98%, and >92% for SARS-CoV-2, *Mycobacterium tuberculosis* (causative agent of TB), and influenza A, respectively, using the Z values given in Table 1 and assuming a residence time of 0.08 s, which was calculated by taking the length of the chamber divided by the bulk velocity.

Table 2. Average irradiance S (mW/cm^2) in a single UVC chamber passage of 10 cm height of Figure 5.

Distance from Top LED Plate (cm)	Irradiance by Top LED Plate	Irradiance by Bottom LED Plate	Total Irradiance
1	9.82	3.52	13.34
2	8.38	3.98	12.36
3	7.34	4.48	11.82
4	6.47	5.06	11.53
5	5.72	5.72	11.44
6	5.06	6.47	11.53
7	4.48	7.34	11.82
8	3.98	8.38	12.36
9	3.52	9.82	13.34

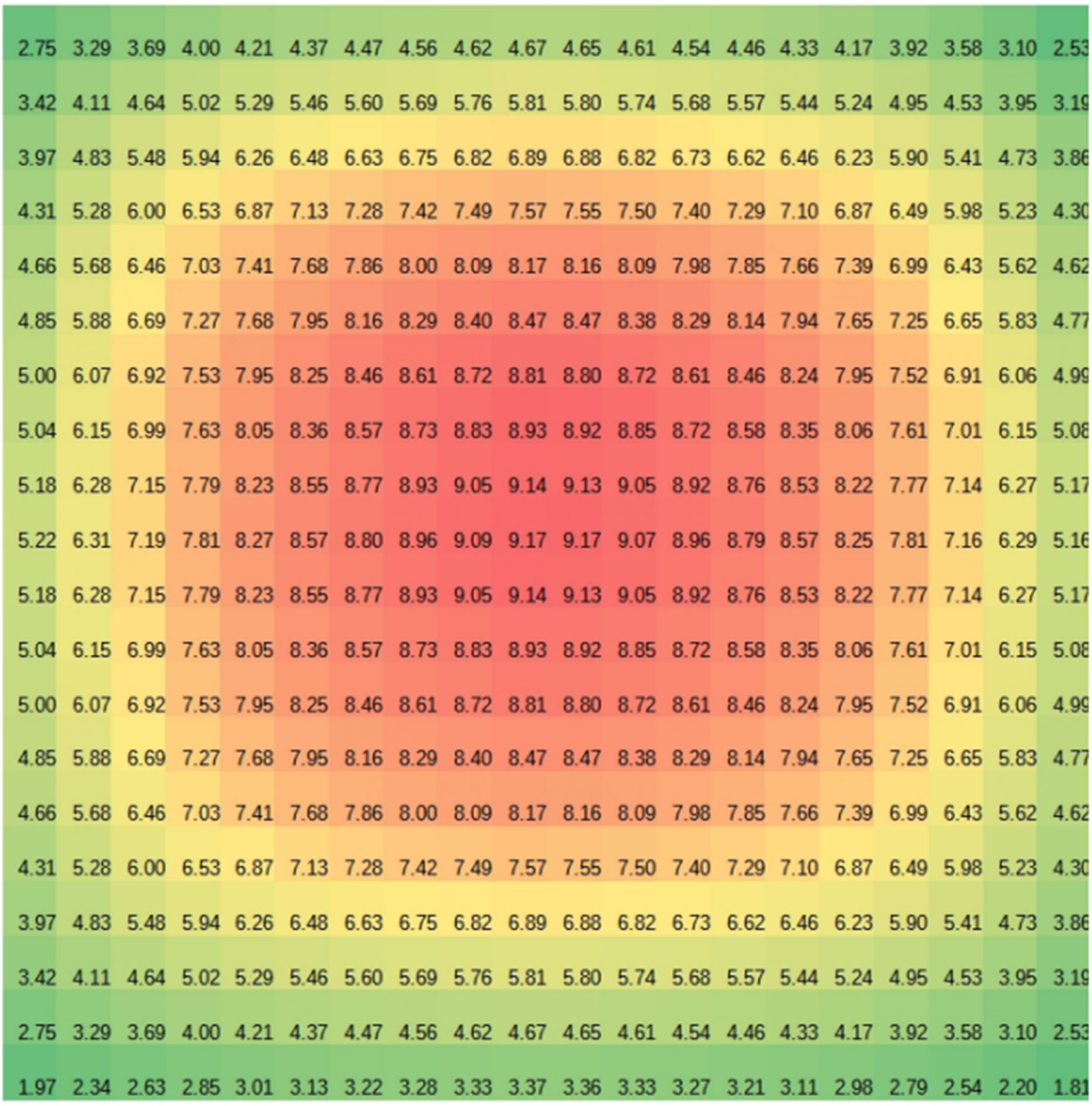

(**a**)

Figure 5. *Cont*.

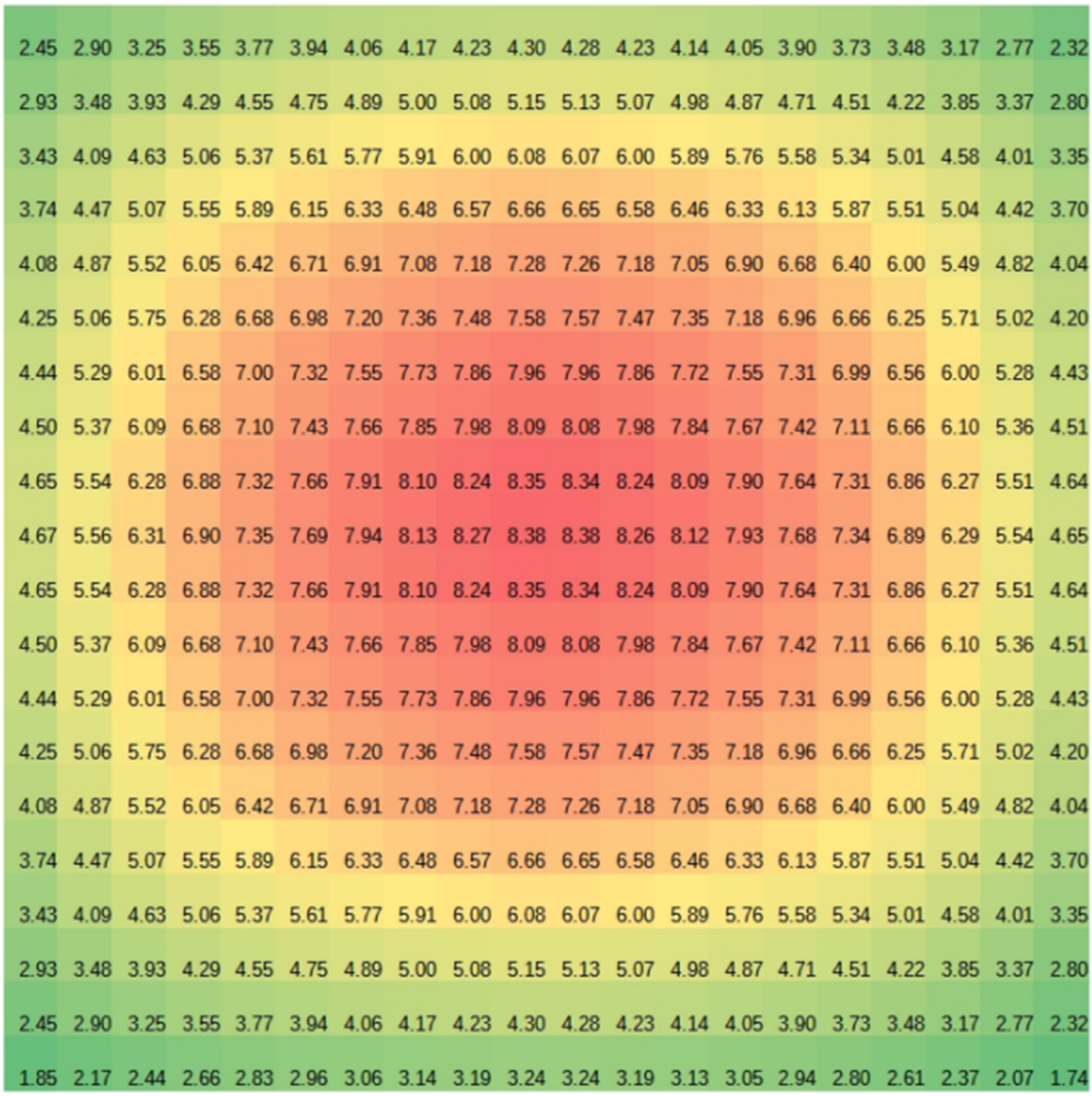

(**b**)

Figure 5. The irradiance S (mW/cm^2) at a horizontal plane of (20, 20) cm as emitted by the upper LED array with the LEDs arrangement of Figure 5b, where the plane is (**a**) 4 cm and (**b**) 6 cm away from the upper LEDs array.

The variations in the irradiance levels seen in Figure 5 illustrate the need for well-mixed air for proper irradiance exposure for all particles. This is achieved by the novel turbulence-generating grid (Figure 6), where the variations between the sharp and rounded corners of the large openings, as well as the slots, increase the turbulence level. As the grid solidity is less than 50%, the estimated pressure drop Δp_g = ~9 Pa using Equation (3), where the CFD gives Δp_g = ~17 Pa because of the enhanced turbulence. This is still much lower than the pressure drop of the dust filter Δp = 120 Pa, assumed for the dust-filter assembly simulation in the CFD computations of Figures 6–9.

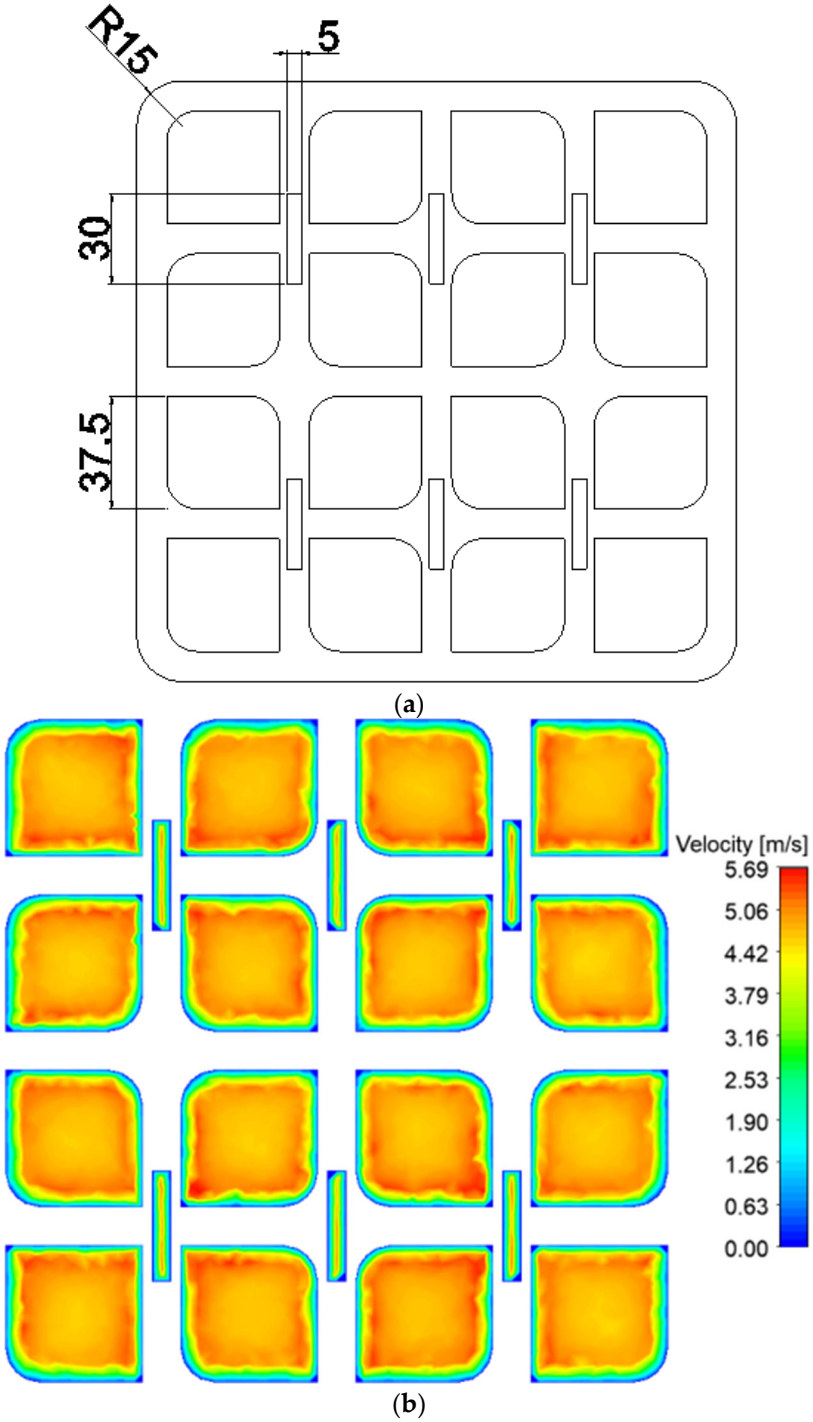

Figure 6. (**a**) The geometry of the turbulence-generating grid, where the given dimensions are in mm and the overall dimensions are (200, 200) mm. (**b**) The time-averaged velocity magnitude field at the grid.

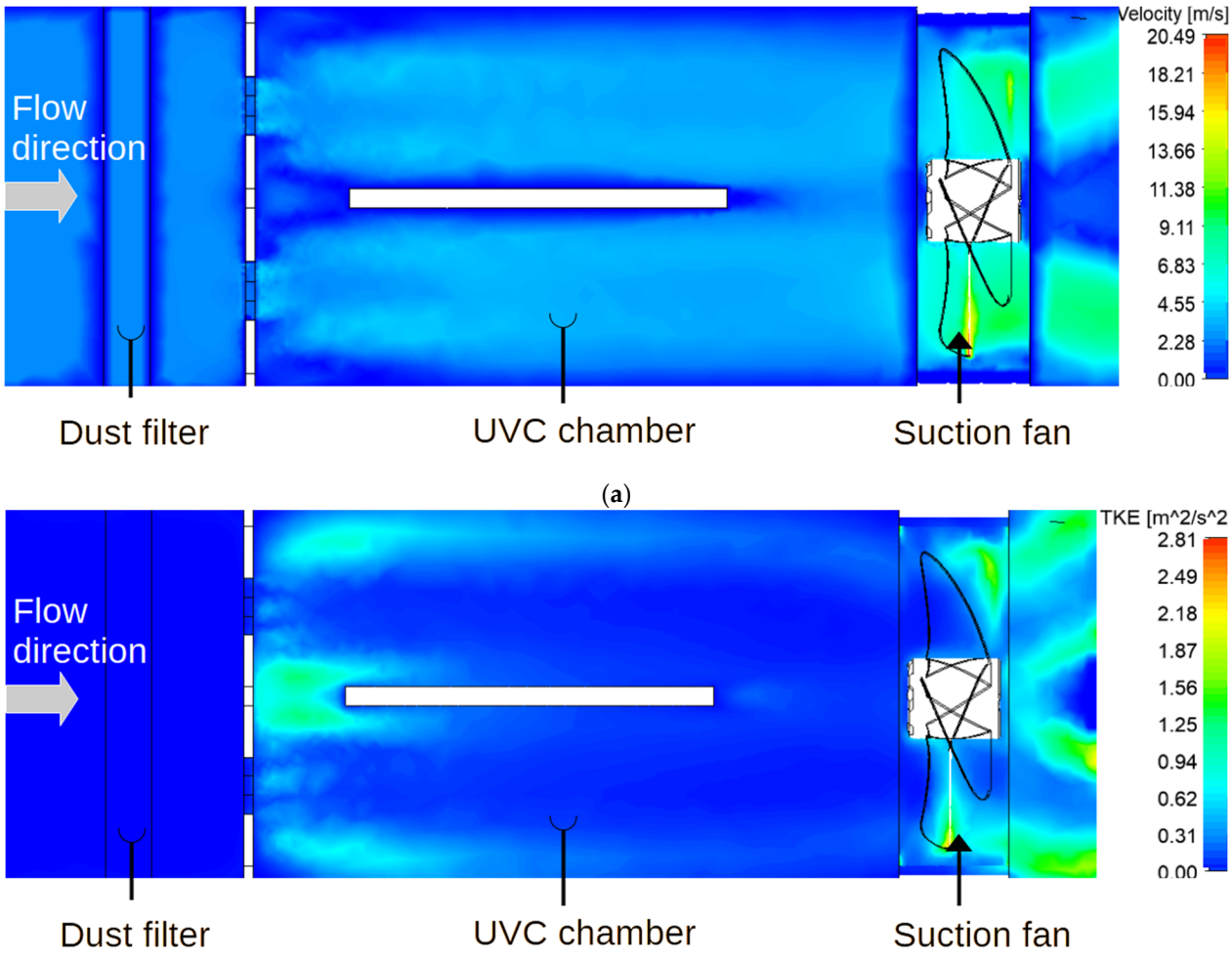

Figure 7. The (**a**) time-averaged velocity magnitude and (**b**) turbulent kinetic energy fields at the mid-spanwise plane of the air purifier.

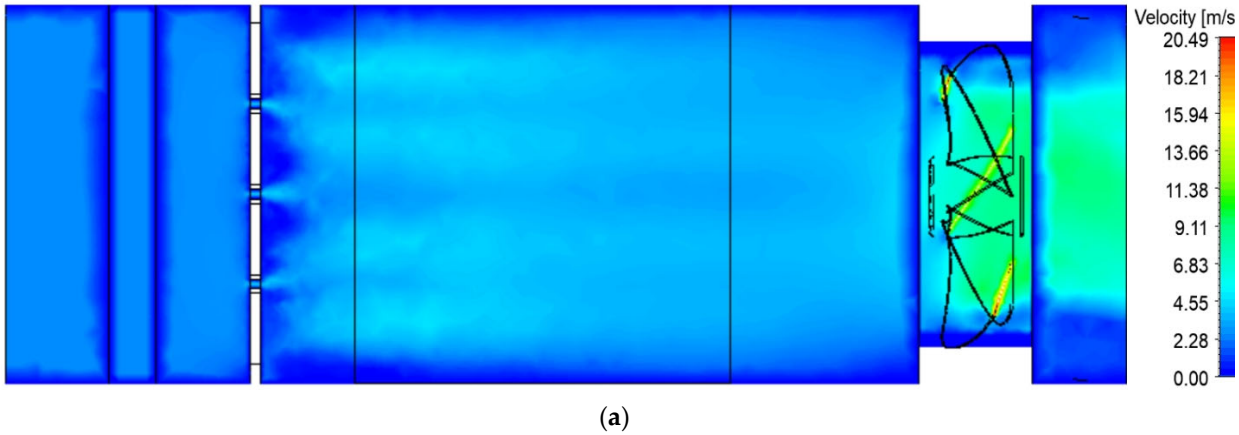

Figure 8. *Cont.*

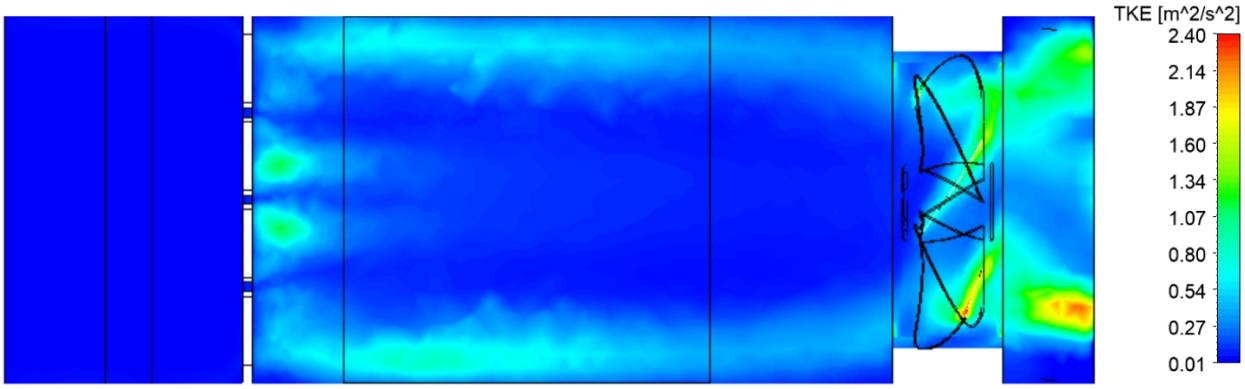

(**b**)

Figure 8. The (**a**) time-averaged velocity magnitude and (**b**) turbulent kinetic energy fields at the mid-vertical plane of the upper UVC chamber.

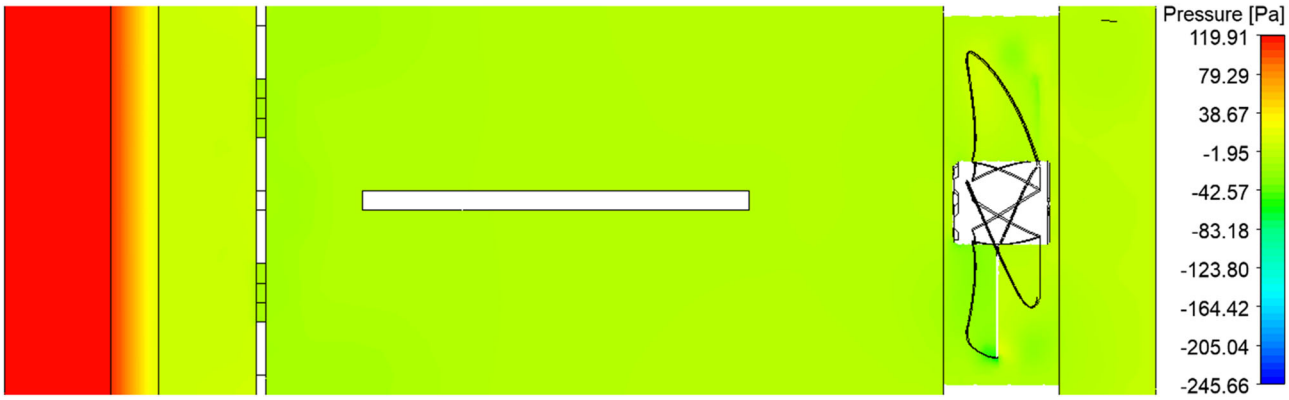

Figure 9. The pressure field at the mid-spanwise plane of the air cleaner and relative to the pressure at a central point after the dust filter.

The velocity on the turbulence-generating grid is up to 5.5 m/s, with closely uniform distributions inside the grid's holes allowing the sufficient flow rate, as seen in Figure 6b. Typical velocity and turbulent kinetic energy (TKE) fields inside the UVC chamber are shown in Figure 7. High TKE levels are seen in low-velocity zones, which capture and then throw fine particles away from those zones. This is while, in other zones, the turbulence intensity is between 20% to 10%, as typical for fully developed turbulent channel flow [39], thus having well-mixed air as needed. One should also note that the Reynolds number based on the hydraulic diameter of the device's cross-section of 0.2×0.2 m^2 is 3.38×10^4 and is 2.24×10^4 when based on the hydraulic diameter of one of the UVC's chambers. Both Reynolds numbers are well within the turbulent range of a non-circular pipe flow [32].

In order to further assess whether the TKE levels illustrated in Figure 7 are sufficient for the well-mixing of the air so all particles receive similar doses of UVC, one can invoke the assumption of frozen turbulence when estimating the particle's motion. It is assumed that the time scale of the particle's motion is much smaller than the integral time scale of the turbulence flow, and such an assumption has been commonly used to investigate the motion of pathogens in larger spaces, e.g., classrooms and hospital wards [40,41]. As a first-order approximation, we also assume isotropic turbulence, yielding that the standard deviation in the vertical particle motion is about $u' \times t$ where u' is the velocity fluctuation, where gravitational effects are neglected because of the small size of the particles [42]. Estimating $u' \simeq \sqrt{2 * TKE/3}$ and taking t = 0.08 s yields a standard deviation of about 6.5 cm in the particle's vertical location for TKE = 1 m^2/s^2 during its motion in one of the

UVC chambers that has a vertical width of 10 cm. This yields a sufficient uniform UVC exposure when considering the total irradiance field values noted in Table 2.

Similarly, one can estimate that the standard deviation of the particle's spanwise motion is also about 6.5 cm. This yields a good particle exchange between the zones of the higher and lower levels of UVC, as illustrated in Figure 5. However, the variation in the UVC levels in the spanwise direction is larger than that in the vertical direction. This calls for the use of reflecting paint on the inner walls of the UVC chambers, which will moderate that variation, as also outlined in the Conclusions section. Nevertheless, Figure 8a shows a rather uniform velocity distribution in the spanwise direction of the UUVC chamber, except toward the side walls, where there is high TKE, according to Figure 8b. Thus, the particles near the side walls have a sufficiently large standard deviation in the spanwise location that will push them toward the center of the UVC chamber, where the UVC irradiation level is higher. This is while particles starting from the central part of the UVC chamber have a lower standard deviation in the spanwise location and, hence, keep their paths more in that central part of higher UVC irradiation level, supporting overall an effective UVC disinfection operation.

Finally, the modeling of the fan can be noticed in both Figures 7 and 8, leading to high speed on its blades and high TKE at its wake. It has been modeled to overcome the pressure gradient that is mostly created by the dust filter, as illustrated in Figure 9 of a pressure field contour plot for the device's mid-spanwise plane. The dust filter on the left of the device causes about a 120 Pa pressure loss, followed by about a 17 Pa loss due to the turbulence-generating grid, where the rest of the pressure losses are caused by turbulent boundary layer losses. One should also note the sharp variation in the pressures around the fan and, hence, the fan acting as a dipole noise source and the need to mitigate fan noise through fan and nozzle designs. This topic is not considered in this study, but the interested reader can be referred to reference [43] for one possible way of reducing the blade profile's self-noise by an aerodynamic redesign.

In the study presented here, we concentrate on the optimization of the competing demands of (i) maximizing the air flow rate through the device; (ii) maximizing the air disinfection efficacy; and (iii) minimizing power consumption. This represents a major engineering challenge, which we attempt to solve by promoting turbulence and good air mixing within the UV chambers, so that all pathogens in the air receive an optimum UV irradiation dose, with none receiving a minimal dose, as is the case if the flow were laminar. Our analysis shows that by introducing turbulence in the airflow, it is possible to produce a UVC-LED device that can achieve >97% inactivation for SARS-CoV-2 and *Mycobacterium tuberculosis* while maintaining a flow rate of 100 L/s and overall power consumption of less than 300 W. While this is promising, we are nonetheless aware that the work presented here is purely theoretical and not based microbiological testing of the device. This is a major limitation of the work presented here, and future work is required to evaluate how the device performs with various microbiological challenges in real life. Notwithstanding, such is the current body of evidence regarding UV inactivation of airborne pathogens, in which we can be confident the device is likely to be effective, provided particles can be exposed to the required minimum UV dose.

4. Conclusions

In this study, we introduce the conceptual design for a low-energy UVC-LED air cleaner aimed at low- and medium-income countries. Through a novel turbulence-generating grid used to enhance the air mixing in the UV irradiance chambers, we achieve >97% inactivation of SARS-CoV-2 and *Mycobacterium tuberculosis* while maintaining a flow rate of 100 L/s and an overall power consumption of <300 W. The turbulence levels generated in the UVC chambers are analyzed using the assumptions of frozen and isotropic turbulence to give estimates for the standard deviations of the small particles, pointing to sufficient uniform UVC irradiation exposure.

The design presented here Is conceptual only, and it is anticipated that further improvement using reflective paint on the walls will enhance the irradiation process. Higher fidelity calculations can be pursued by coupling a radiance transport equation approximation with CFD and particle dynamics while analyzing the LED heat transfer. This will confirm the UVC exposure of the particles to be sufficiently uniform and highlight if there are any further power losses due to heat transfer issues that are not considered in this feasibility study. Fan noise considerations should also be included. The device should also be experimentally tested, and further consideration can be given to environmental conditions affecting the pathogen transmissibility [11]. These steps are planned to be taken in the future.

Author Contributions: Conceptualization, E.J.A., N.V., A.S. and C.B.B.; Methodology, E.J.A., T.S., L.C.-G., F.M., A.S. and C.B.B.; Software, C.B.B.; Validation, T.S. and L.C.-G.; Formal analysis, S.K., D.R., T.S. and L.C.-G.; Investigation, S.K., D.R., E.J.A., N.V., F.M., A.S. and C.B.B.; Resources, E.J.A., N.V. and A.S.; Data curation, S.K., D.R., T.S. and L.C.-G.; Writing—original draft, E.J.A.; Writing—review & editing, N.V., A.S. and C.B.B.; Visualization, S.K., D.R., T.S. and L.C.-G.; Supervision, E.J.A., N.V., F.M., A.S. and C.B.B.; Project administration, S.K., E.J.A., N.V. and F.M.; Funding acquisition, E.J.A., N.V., A.S. and C.B.B. All authors have read and agreed to the published version of the manuscript.

Funding: This study was supported by the UK Royal Academy of Engineering grant EXPP2021\1\247.

Data Availability Statement: The data presented in this study are further available on request from the corresponding author. Further data will be publicly available by the end of this project.

Acknowledgments: The assistance of Maham Sandhu of Queen Mary University of London, UK, and Rishav Raj of IIT Madras India in terms of project resources, administration, and preliminary discussions is kindly acknowledged. This study was supported by the UK Royal Academy of Engineering grant EXPP2021\1\247.

Conflicts of Interest: The authors declare no conflict of interest.

Appendix A. Dust-Filter Efficiencies

The total single filter efficiency (SFE) E_{T} is calculated as [29]

$$E_T = 1 - (1 - E_D)(1 - E_R)(1 - E_I) \tag{A1}$$

The diffusion SFE E_{D} is very small for our filter and thus neglected. Its calculation procedure can be found in [30]. The interception SFE E_{R} can be calculated as

$$E_R = \frac{1 - \alpha_f}{K}\left(\frac{R^2}{1 + R}\right) \tag{A2}$$

where α_f is the fiber solidity and

$$K = \alpha_f - \frac{\alpha_f^2}{4} - \frac{ln\alpha_f}{2} - \frac{3}{4} \tag{A3}$$

where R is the ratio between the particle's diameter to the fiber's diameter, i.e., $R = d_{\mathrm{p}}/d_{\mathrm{f}}$. Equation (A3) is considered to be accurate for $R < 0.2$.

The inertial impaction SFE E_{I} is taken as

$$E_I = \frac{J * St}{2K^2} \tag{A4}$$

where

$$J = \begin{cases} \left(29.6 - 28\alpha_f^{0.62}\right)R^2 - 27.5R^{2.8} & , R < 0.4 \\ 2 & , R > 0.4 \end{cases} \tag{A5}$$

The Stokes number St is

$$St = \frac{d_p^2 \rho_p U_0}{18 d_p \mu} \quad \text{(A6)}$$

where the slip factor is taken as one because the particle diameter d_{p} is on the micron scale and ρ_p is the particle density assumed as of fresh water. Equation (A5) is considered an accurate approximation when the fibrous filter's solidity is in the range of $0.0035 < \alpha_f < 0.111$, which agrees with our dust filter of $\alpha_f = 0.05$.

References

1. Zhang, R.; Li, Y.; Zhang, A.L.; Wang, Y.; Molina, M.J. Identifying airborne transmission as the dominant route for the spread of COVID-19. *Proc. Natl. Acad. Sci. USA* **2020**, *117*, 14857–14863. [CrossRef]
2. Miller, S.L.; Nazaroff, W.W.; Jimenez, J.L.; Boerstra, A.; Buonanno, G.; Dancer, S.J.; Kurnitski, J.; Marr, L.C.; Morawska, L.; Noakes, C. Transmission of SARS-CoV-2 by inhalation of respiratory aerosol in the Skagit Valley Chorale superspreading event. *Indoor Air* **2021**, *31*, 314–323. [CrossRef] [PubMed]
3. Beggs, C.B.; Noakes, C.J.; Sleigh, P.A.; Fletcher, L.A.; Siddiqi, K. The transmission of tuberculosis in confined spaces: An analytical review of alternative epidemiological models. *Int. J. Tuberc. Lung Dis.* **2003**, *7*, 1015–1026. [PubMed]
4. Escombe, A.R.; Moore, D.A.; Gilman, R.H.; Navincopa, M.; Ticona, E.; Mitchell, B.; Noakes, C.; Martinez, C.; Sheen, P.; Ramirez, R.; et al. Upper-room ultraviolet light and negative air ionization to prevent tuberculosis transmission. *PLoS Med.* **2009**, *6*, e1000043. [CrossRef]
5. Bloch, A.B.; Orenstein, W.A.; Ewing, W.M.; Spain, W.H.; Mallison, G.F.; Herrmann, K.L.; Hinman, A.R. Measles outbreak in a paediatric practice: Airborne transmission in an office setting. *Paediatrics* **1985**, *75*, 676–683. [CrossRef]
6. Yan, J.; Grantham, M.; Pantelic, J.; Bueno de Mesquita, P.J.; Albert, B.; Liu, F.; Ehrman, S.; Milton, D.K.; Emit Consortium. Infectious virus in exhaled breath of symptomatic seasonal influenza cases from a college community. *Proc. Natl. Acad. Sci. USA* **2018**, *115*, 1081–1086. [CrossRef]
7. Houben, R.M.; Dodd, P.J. The global burden of latent tuberculosis infection: A re-estimation using mathematical modelling. *PLoS Med.* **2016**, *13*, e1002152. [CrossRef] [PubMed]
8. World Health Organisation. *Global Tuberculosis Report 2021*; WHO: Geneva, Switzerland, 2021.
9. Greenhalgh, T.; Jimenez, J.L.; Prather, K.A.; Tufekci, Z.; Fisman, D.; Schooley, R. Ten scientific reasons in support of airborne transmission of SARS2-CoV-2. *Lancet* **2021**, *397*, 1603–1605. [CrossRef] [PubMed]
10. Beggs, C.B.; Avital, E.J. Upper-room ultraviolet air disinfection might help to reduce COVID-19 transmission in buildings: A feasibility study. *PeerJ* **2020**, *8*, 10196. [CrossRef]
11. Beggs, C.B.; Avital, E.J. A psychometric model to assess the biological decay of the SARS-CoV-2 virus in aerosols. *PeerJ* **2021**, *9*, 11024. [CrossRef]
12. Seminara, G.; Carli, B.; Forni, G.; Fuzzi, S.; Mazzino, A.; Rinaldo, A. Biological fluid dynamics of airborne COVID-19 infection. *Rend. Lincei. Sci. Fis. Nat.* **2020**, *31*, 505–537. [CrossRef]
13. Morawska, L.; Tang, J.W.; Bhanfleth, W.; Bluyssen, P.M.; Boerstra, A.; Buonanno, G.; Cao, J.; Dancer, S.; Floto, A.; Franchimon, F.; et al. How can airborne transmission of COVID-19 indoors be minimised? *Environ. Int.* **2020**, *142*, 105832. [CrossRef] [PubMed]
14. Xie, X.; Li, Y.; Chwang, A.T.; Ho, P.L.; Seto, W.H. How far droplets can move in indoor environments–revisiting the Wells evaporation-falling curve. *Indoor Air* **2007**, *17*, 211–225. [CrossRef] [PubMed]
15. Stadnyski, V.; Bax, C.F.; Bax, A.; Anfinrud, P. The airborne lifetime of small speech droplets and their potential importance in SARS2-CoV-2 transmission. *Proc. Natl. Acad. Sci. USA* **2020**, *117*, 11875–11877. [CrossRef] [PubMed]
16. Anghel, L.; Popovici, C.G.; Statescu, C.; Sascău, R.; Verde, M.; Ciocan, V.; Șerban, I.-L.; Mărănducă, M.A.; Hudi, S.-V.; Țurcanu, F.-E. Impact of HVAC-System on the dispersion of infectious aerosols in a cardiac intensive care unit. *Int. J. Environ. Res. Public Health* **2020**, *17*, 6582. [CrossRef] [PubMed]
17. Beggs, C.B.; Shepherd, S.J.; Kerr, K.G. Potential for airborne transmission of infection in the waiting areas of healthcare premises: Stochastic analysis using a Monte Carlo model. *BMC Infect. Dis.* **2010**, *10*, 247. [CrossRef] [PubMed]
18. Butler, M.B.; Sloof, D.; Peters, C.; Gouliouris, T.; Thaxter, R.; Keevil, V.L.; Beggs, C.B. Impact of supplementary air filtration on aerosols and particulate matter in a UK hospital ward: A case study. *J. Hosp. Infect.* **2023**. online ahead of print. [CrossRef]
19. Beggs, C.B. A quantitative method for evaluating the photoreactivation of ultraviolet damaged microorganisms. *Photochem. Photobiol. Sci.* **2002**, *1*, 431–437. [CrossRef]
20. First, M.W.; Nardell, E.A.; Chaisson, W.; Riley, R. Guidelines for the application of upper-room ultraviolet germicidal irradiation for preventing transmission of airborne contagion-Part I: Basic principles. *Tran-Am. Soc. Heat. Refrig. Air-Cond. Eng.* **1999**, *105*, 869–876.
21. Davidson, B.L. Bare-bulb upper-room germicidal ultraviolet-c (GUV) indoor air disinfection for COVID-19. *Photochem. Photobiol.* **2021**, *97*, 524–526. [CrossRef]
22. Qjao, Y.; Yang, M.; Marabella, I.A.; McGee, D.A.J.; Aboubakr, H.; Goyal, S.; Hogan, C.J., Jr.; Olson, B.A.; Torremorell, M. Greater then 3-Log reduction in viable coronavirus aerosol concentration in ducted Ultraviolet-C (UV-C) Systems. *Environ. Sci. Technol.* **2021**, *55*, 4174–4182.

23. Cullen, A.P. Photokeratitis and other phototoxic effects on the cornea and conjunctiva. *Int. J. Toxicol.* **2002**, *21*, 455–464. [CrossRef] [PubMed]
24. Harrison, G.I.; Young, A.R. Ultraviolet radiation-induced erythema in human skin. *Methods* **2002**, *28*, 14–19. [CrossRef] [PubMed]
25. Burridge, H.C.; Bhagat, R.K.; Stettler, M.E.; Kumar, P.; De Mel, I.; Demis, P.; Hart, A.; Johnson-Llambias, Y.; King, M.-F.; Klymenko, O.; et al. The ventilation of buildings and other mitigating measures for COVID-19: A focus on wintertime. *Proc. R. Soc. A* **2021**, *477*, 20200855. [CrossRef]
26. Inagaki, H.; Saito, A.; Sugiyama, H.; Okabayashi, T.; Fujimoto, S. Rapid inactivation of SARS-CoV-2 with deep-UV LED irradiation. *Emerg. Microbes Infect.* **2020**, *9*, 1744–1747. [CrossRef]
27. World Health Organisation. *Roadmap to Improve and Ensure Indoor Ventilation in the Contextr of COVID-19*; World Health Organisation: Geneva, Switzerland, 2021.
28. Basu, S. Computational characterization of inhaled droplet transport to the nasopharynx. *Sci. Rep.* **2021**, *11*, 6652. [CrossRef] [PubMed]
29. Thomas, D.; Penicot, P.; Contal, P.; Leclerc, D.; Vendel, J. Clogging of fibrous filters by solid aerosol particles experimental and modelling study. *Chem. Eng. Sci.* **2001**, *56*, 3549–3561. [CrossRef]
30. Shou, D.; Fan, J.; Ye, L.; Zhnag, H.; Qian, X.; Zhang, Z. Inverse problem of air filtration of nanoparticles: Optical quality factors of fibrous filters. *J. Nano Mater.* **2015**, *2015*, 1683912. [CrossRef]
31. Kurian, T.; Fransson, J.H.M. Grid-generated turbulence revisited. *Fluid Dyn. Res.* **2009**, *41*, 021403. [CrossRef]
32. Schlichting, H. *Boundary Layer Theory*; McGraw Hill: New York, NY, USA, 2018.
33. Yan, Y.; Avital, E.; Williams, J.; Cui, J. CFD analysis for the performance of micro-vortex generator on aerofoil and vertical axis turbine. *J. Renew. Sustain. Energy* **2019**, *11*, 043302. [CrossRef]
34. Menter, F.R. *Improved Two-Equation k-Omega Turbulence Models for Aerodynamic Flows*; NASA Technical Memorandum TM-103975; Technical Report; NASA: Ames, CA, USA, 1992.
35. Pritchard, D.C. *Lighting*, 6th ed.; Routledge: New York, NY, USA, 1999.
36. Batchelor, G.K. *An Introduction to Fluid Dynamics*; Cambridge University Press: Cambridge, UK, 1992.
37. Southery, A.; Fox, M.; Yeomans, T.; Mitchell, B. A comparison of the characteristics of ISO fine test dust versus real household dust. In Proceedings of the 12th International Conference on Indoor Air Quality and Climate, Austin, TX, USA, 5–10 June 2011.
38. Younis, B.A.; Yang, T.H. Computational modeling of ultraviolet disinfection. *Water Sci. Technol.* **2010**, *62*, 1872–1878. [CrossRef] [PubMed]
39. Kulick, J.D.; Fessler, J.R.; Eaton, S.K. Particle response and turbulence modification in fully developed channel flow. *J. Fluid Mech.* **1994**, *277*, 109–139. [CrossRef]
40. Abuhegazy, M.; Talaat, K.; Anderoglu, O.; Poroseva, S.V. Numerical investigation of aerosol transport in a classroom with relevance to COVID-19. *Phys. Fluids* **2020**, *32*, 103311. [CrossRef] [PubMed]
41. Gilkeson, C.A.; Noakes, C.J.; Khan, M.A.I. Computational fluid dynamics modelling and optimisation of an upper-room ultraviolet germicidal irradiation system in a naturally ventilated hospital ward. *Indoor Built Environ.* **2014**, *23*, 449–466. [CrossRef]
42. Pope, S.B. *Turbulent Flows*; Cambridge University Press: Cambridge, UK, 2003.
43. Shen, X.; Avital, E.; Zhao, Q.; Gao, J.; Li, X.; Paul, G.; Korakianitis, T. Surface curvature effects on the tonal noise performance of a low Reynolds number aerofoil. *Appl. Acoust.* **2017**, *125*, 34–40. [CrossRef]